RSC Advances

REVIEW

View Article Online
View Journal | View Issue

Cite this: *RSC Adv.*, 2023, **13**, 3265

A review on the synthesis of metal oxide nanomaterials by microwave induced solution combustion

Ziyang Yin, Si Li, Xiang Li, Wuyang Shi, Wei Liu, Zhengxia Gao, Mengya Tao, Chengliang Ma * and Yuan Liu

With the increasing awareness of environmental protection and health, the preparation of metal oxide nanomaterials by environmentally friendly methods is favored by more and more researchers both at home and abroad. The preparation of metal oxide nanomaterials by a microwave-induced solution combustion synthesis method can significantly reduce the reaction time, energy consumption, and the use of toxic chemicals, which is an energy-saving, environmentally friendly method for nanomaterials synthesis. In addition, the microwave-induced solution combustion synthesis (MISCS) method has many advantages such as fast reaction speed, high selectivity, small product size, and homogeneous composition. This paper briefly describes the mechanism of the MISCS and its advantages in the synthesis of metal oxide nanomaterials, the related studies on microwave-induced solution combustion synthesis of metal oxide nanomaterials, and the effects of process parameters on the microstructure and properties of metal oxide nanomaterials synthesized by MISCS. Furthermore, some technical difficulties facing the synthesis of metal oxide nanomaterials by MISCS are summarized, and the future direction has also been prospected.

Received 12th December 2022
Accepted 12th January 2023

DOI: 10.1039/d2ra07936d

rsc.li/rsc-advances

1 Introduction

The concept of nanomaterials first originated in the early 1980s and was proposed by German scientist H. Gleiter.[1] In the late 1980s, this concept gained rapid development and attracted the attention of scientists worldwide. On the basis of this, a lot of research work related to nanomaterials was carried out. Materials that exist in at least one dimension in three-dimensional space with nanoscale dimensions (1–100 nm) or are composed of them as basic units can be called nanomaterials.[2] Compared to ordinary materials, the particle size of nanomaterials is on the order of nanometers. The fine particle size gives rise to corresponding changes in the crystal structure and surface electronic structure of nanomaterials. Therefore, nanomaterials possess many special effects: small size effect,[3] quantum size effect,[4] surface effect,[5] and macroscopic quantum tunneling effect.[6] Due to these special effects, nanomaterials have optical, magnetic, electrical, and thermal properties that are different from those of ordinary materials.[7] These differences enable nanomaterials to have a wide range of applications in catalysts,[8,9] adsorbents,[10,11] antimicrobial agents,[12,13] functional ceramics,[14,15] and flame retardants.[16]

The liquid phase combustion synthesis, also named solution combustion synthesis (SCS) which start to be implemented in 1981 with the Jain method.[17] SCS is a simple, fast, efficient and versatile method. The method can be used to prepare oxide materials with controlled properties (homogeneity and high purity) for a wide number of applications, such as catalysts, solid fuel cells and electronics.[18–22] SCS is based on propellant chemistry and the stoichiometric ratio of oxidant to fuel. It involves an exothermic reaction between metal nitrate (oxidant) and organic fuel. The solution combustion synthesis method consists of three main steps: (1) formation of combustion mixture, (2) formation of gel and (3) combustion of gel. Most metal oxides can be obtained by reacting metal nitrates with fuel. Nitrates are the preferred metal precursors because they provide water/alcohol soluble metal ions and ensure homogeneity.

According to the different ignition modes, the solution combustion synthesis method can be divided into the traditional solution combustion synthesis method and the microwave-induced solution combustion synthesis method. The traditional solution combustion synthesis method transfers heat from the outside to the inside of the material by means of heat conduction. This heat transfer mechanism leads to a certain temperature gradient in the material, which leads to the formation of different crystalline phases and the growth of particles. Microwave induced solution combustion synthesis is a new method of nanomaterials preparation based on

Henan Key Laboratory of High Temperature Functional Ceramics, School of Material Science and Engineering, Zhengzhou University, 75 Daxue Road, Zhengzhou 450052, China. E-mail: machengliang@zzu.edu.cn

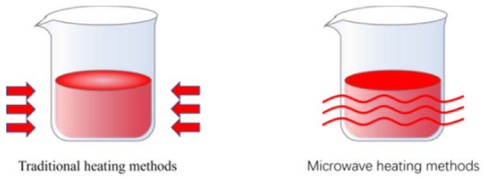

Fig. 1 The schematic of the two different heating modes.

traditional solution combustion synthesis. The synthesis method has a different heating mechanism than the conventional solution combustion synthesis method. Microwave-induced solution combustion is mainly due to the rapid oscillation of molecular dipoles in the presence of microwaves. This oscillation leads to a higher molecular collision rate, which generates more heat.[23] Due to its unique heating mechanism, the microwave heating allows for volumetric heating of the material, resulting in a more uniform heat distribution within the material.[24] In addition, the microwave-induced solution combustion synthesis method can rapidly prepare a wide variety of nanomaterials with excellent physicochemical properties. Fig. 1 shows the schematic of the two different heating modes.

Nowadays, a wide variety of equipment for microwave-assisted reaction synthesis exists in chemical synthesis laboratories. In the early days of microwave synthesis, the main chemical synthesis reactions were carried out in home microwave ovens. The equipment is cheap and convenient, but the parameters of the reaction process were precisely unknown, such as the reaction temperature, the pressure inside the reaction vessel and the power of the microwave.[25] Due to these uncertainties, the control of the safety and reproducibility of the synthesis process has become particularly important. Therefore, it is necessary to use an advanced microwave reaction system. This system needs to be equipped with various probes and sensors to monitor the temperature and pressure inside the reaction vessel. The devices can avoid the hazards of high temperature and pressure caused by the violent reaction of solvents in the closed reaction vessel. A schematic diagram of the microwave-assisted reactor system is shown in Fig. 2. The microwave device will provide uniform heating of the entire reactant system. In addition, a temperature sensor and a pressure sensor are inserted in the reaction vessel to monitor the temperature and pressure inside the reaction vessel, respectively.[23]

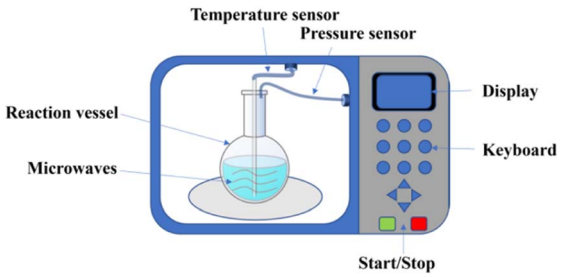

Fig. 2 Schematic illustration of the microwave reactor system for microwave assisted synthesis.

2 Microwave-induced solution combustion synthesis method

In microwave chemistry, the microwave heating mechanism is based on the "microwave dielectric heating" effect for efficient heating of materials. This phenomenon depends on the ability of a particular raw material (oxidant or organic fuel) to absorb microwave energy and convert it into heat.[26] Microwave-induced solution combustion is induced by two main mechanisms of heating: dipole polarization and ionic conductivity.[27] When the MW field is applied, the dipole and polar units of the reactants in the reaction mixture try to align with the microwave electric field frequency, and the dipoles constantly try to realign the oscillating electric field.[28] This type of process leads to molecular friction and dielectric loss, which results in energy loss in the form of heat. The heat generated by this process is directly related to the ability of the substrate itself to align with the microwave field frequency. If the dipole does not have enough time to rearrange under the action of the microwave electric field, or cannot reorient quickly with the microwave field, the phenomenon of heating will not occur. The electric field oscillations of 2.45 GHz lead to the rotation of many polar molecules in the liquid, resulting in resistive heating in the medium (dielectric loss).[29]

When microwave electric field is applied, the charged particles dissolved in the reaction mixture oscillate back and forth in response to the applied MW electric field and collide with neighboring molecules, thus generating heat. The heat generated under the ion conduction mechanism is much higher than that generated under the dipole polarization mechanism. The reaction mixtures consisting of free ions exhibit transient heating, which is important for the preparation of nanostructures in ionic liquids.[30] The heating characteristics of the reacting material under microwave radiation conditions depend on its dielectric properties. The dielectric properties of a material are mainly determined by two parameters: (1) the dielectric constant ε'' (the ability of the material to be polarized by the applied electric field) and (2) the dielectric loss ε' (the ability of the material to dissipate thermal energy by converting the absorbed MW energy into heat).[31] The ability of a given substance to convert electromagnetic energy into thermal energy at a given frequency and temperature is determined by the so-called loss factor $\tan\delta = \varepsilon''/\varepsilon'$. In general, solvents can be classified according to their loss factor as high absorbing ($\tan\delta > 0.5$), medium absorbing ($\tan\delta = 0.1$–0.5) and low absorbing ($\tan\delta < 0.1$).[26]

The microwave-induced solution combustion synthesis method is also called microwave-assisted solution combustion synthesis method. Fig. 3 shows the synthetic route of microwave-induced solution combustion method. Firstly, inorganic metal salts, deionized water, and fuel are prepared into a mixed solution. Then the mixed solution is dissolved on a magnetic stirrer until it is well mixed to obtain the precursor

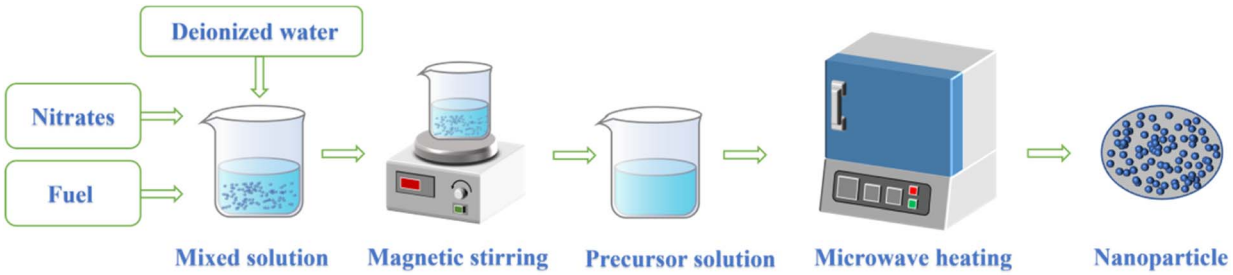

Fig. 3 Diagram of microwave induced combustion synthesis.

solution. Finally, the precursor solution was placed in a microwave oven for microwave heating to form the nanomaterials. In the process of solution combustion, the whole combustion phase only lasts for a few minutes. Besides, the inorganic metal salts in the reactants are mainly used as oxidants, and the fuel and its decomposition products are mainly used as reducing agents, while microwaves play the role of inducing redox reactions. In the process of microwave-induced combustion synthesis, nitrates of metals are often used as oxidants while urea ($CO(NH_2)_2$), citric acid ($C_6H_8O_7$), glycine ($C_2H_5NO_2$), and plant extracts commonly are often used as fuels.[24]

3 Microwave-induced combustion synthesis of nanomaterials

3.1 Single metal oxide nanomaterials

The microwave-induced solution combustion synthesis has the advantages of short heating time, uniform heating, and high purity. Therefore, this approach can be used to rapidly prepare high purity single metal oxide nanomaterials. At present, researchers have synthesized various kinds of single metal oxide nanomaterials by microwave-induced solution combustion, and the prepared nanomaterials have been applied in various fields. Table 1 lists some relevant reports on the synthesis of single metal oxide nanomaterials by microwave induced solution combustion. Patra *et al.* group used $Mn(NO_3)_2$ as oxidant and $C_2H_5NO_2$ as fuel to prepare Mn_3O_4 with high specific capacitance and small particle size using microwave induced combustion synthesis method. These Mn_3O_4 nanoparticles can operate over a wide range of potentials and are inherently environmentally friendly. Therefore, The mixed Mn_3O_4 NPs can be used as an effective electrode material for electrochemical supercapacitors. The average crystallite size of MW synthesized Mn_3O_4 nanoparticles is calculated to be 28.08 nm by using the Debye Scherer equation. Fig. 4 shows that the microstructure is in the form of sponge like aggregates.[32] The single metal oxide nanomaterials prepared by microwave-induced combustion synthesis have small particle sizes and high specific surface area, which can be used as antibacterial agents and adsorbents with efficient antibacterial properties and adsorption capacity.

Anand *et al.* group successfully prepared CuO nanoparticles by microwave-induced combustion synthesis using copper

Table 1 Microwave induced solution combustion synthesis single metal oxide nanomaterials

Synthetic materials	Raw materials	Material characteristics	Particle/ crystallite size (nm)	Applications
Mn_3O_4	$Mn(NO_3)_2 \cdot 4H_2O$ $C_2H_5NO_2$	High crystallinity Excellent capacitance High purity	28.08	Electrode material[32]
CuO	$Cu(NO_3)_2$ *Moringa oleifera* and pomegranate leaves	Small particle size High crystallinity	14.82/15.82	Antibacterial agent[33]
MgO	$Mg(NO_3)_2 \cdot 6H_2O$ $C_2H_5NO_2$	Small particle size High porosity	18	Adsorbent[34]
Nb_2O_5	NH_4 $[NbO(C_2O_4)_2\text{-}(H_2O)_2](H_2O)$ NH_4NO_3 $CO(NH_2)_2/C_6H_8O_7$	High crystallinity Small particle size High purity	5–110	Photocatalysis[35]
ZnO	$Zn(NO_3)_2$ fruit, seed, and pulp extracts of *C. colocynthis*	Desirable antioxidant High antibacterial activity	27–85	Antibacterial agent[36]
Fe_3O_4	$Fe(NO_3)_3 \cdot 9H_2O$ $C_6H_8O_7$	Small particle size High saturation magnetization strength	22–30	Magnetic resonance imaging[37]
Al_2O_3	$Al(NO_3)_3 \cdot 9H_2O$ $CO(NH_2)_2$	Small particle size High specific surface area	30–40	Catalytic support[38]
CeO_2	$Ce(NO_3)_4$ $CO(NH_2)_2$	High crystallinity High purity	18.23–23.83	Catalyst[39]

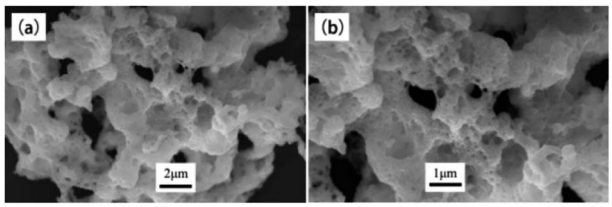

Fig. 4 The SEM image of Mn_3O_4 nanoparticles [reprinted with permission from ref. 32. Copyright 2021 Elsevier].

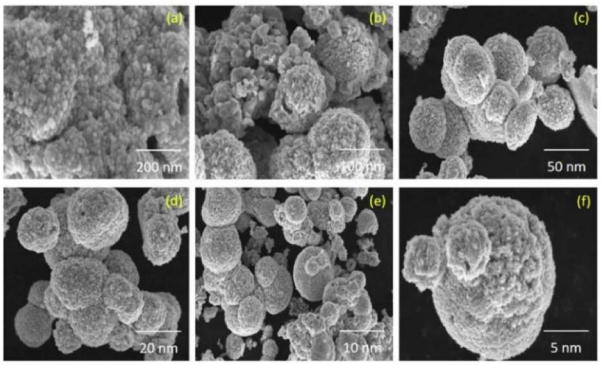

Fig. 5 The SEM images of CuO NPs synthesized: (a–c) *Moringa oleifera*, (d–f) *Punica granatum* [reprinted with permission from ref. 33. Copyright 2021 Elsevier].

nitrate as oxidant and *Moringa oleifera* or *Punica granatum* extracts as fuel. The crystallization properties of CuO nanoparticles were studied by X-ray diffraction. It was found that the average grain size of CuO nanoparticles prepared with *Moringa oleifera* extract as fuel was 18.42 nm and the average grain size of CuO nanoparticles prepared using *Punica granatum* extract as fuel was 15.82 nm. The SEM images showed that the morphology of CuO NPs synthesized using *Moringa oleifera* and *Punica granatum* was spherical with an average grain size between 12–18 nm, which is in agreement with the powder XRD results. Fig. 5 shows that the spherical shape of nano-CuO. In addition, the antibacterial activity of the copper oxide nanoparticles prepared by the method was studied. The results showed that the copper oxide nanoparticles prepared by this method can be used to cure urinary tract infections.[33] Priyadarshini *et al.* group synthesized cubic MgO nanoparticles with a grain size of 18 nm by microwave induced combustion synthesis, which can be used as an adsorbent to efficiently remove organic dyes from wastewater. The FESEM analysis showed the aggregation of small rod-like structured MgO particles with grain size in the range of 60–85 nm.[34]

In the microwave induced solution combustion process, a series of process parameters such as microwave power, oxidant-to-fuel dosage ratio, type of fuel, and pH value of the precursor solution play a decisive role in the structure and properties of the products. Luiz *et al.* group successfully prepared Nb_2O_5 powder. The effect of the amount of ammonium niobium oxalate and urea on the particle size of the product was studied. The results showed that when the oxidant-

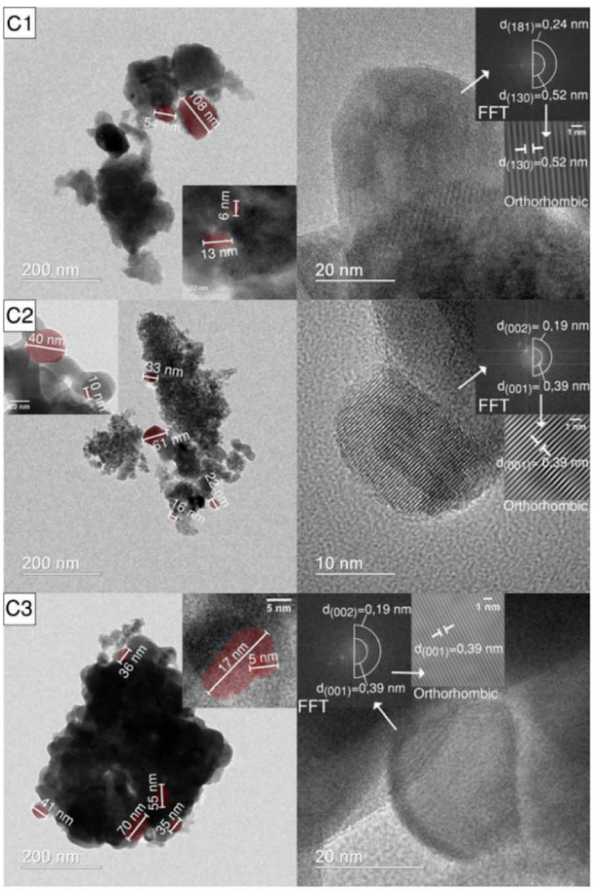

Fig. 6 TEM (left) and HRTEM (right) images of the C1, C2 and C3 samples: (C1) stoichiometric, (C2) excess oxidant, (C3) excess fuel [reprinted with permission from ref. 35. Copyright 2021 doiSerbia].

to-fuel ratio is stoichiometric, Nb_2O_5 with larger particle size is produced, while Nb_2O_5 with smaller particle size is obtained with either excess fuel or excess oxidant. This is mainly because the amount of oxidant and fuel can change the reaction synthesis temperature, which affects the size of the resulting particles. The TEM and XRD analyses were consistent. In Fig. 6, the TEM results confirmed that the diameters of the obtained niobium pentoxide (Nb_2O_5) nanoparticles were in the range of 5–110 nm. The HRTEM images of C1 samples showed the presence of orthogonal crystal structures with planar spacing of 0.52 nm and 0.24 nm, corresponding to (130) and (181) planes, respectively. Besides, the (002) and (001) planar spacing of C2 and C3 samples were 0.19 and 0.39 nm, respectively.[35]

Azizi *et al.* group synthesized ZnO nanoparticles with mean particle size between 27 and 85 nm by different bio-fuels. The microscopic morphology of the ZnO particles synthesized using fruits, seeds and pulp as fuels were flower-like, hexagonal and block nanostructures, respectively.[36] Radpour *et al.* group synthesized Fe_3O_4 powders by conventional ignition and microwave ignition methods. When $\varphi = 1$, the sample prepared by conventional ignition contains only the Fe_3O_4 phase, while the sample made by microwave ignition contains the Fe_3O_4 phase and some impurity phases such as α-Fe_2O_3 and FeO.[37]

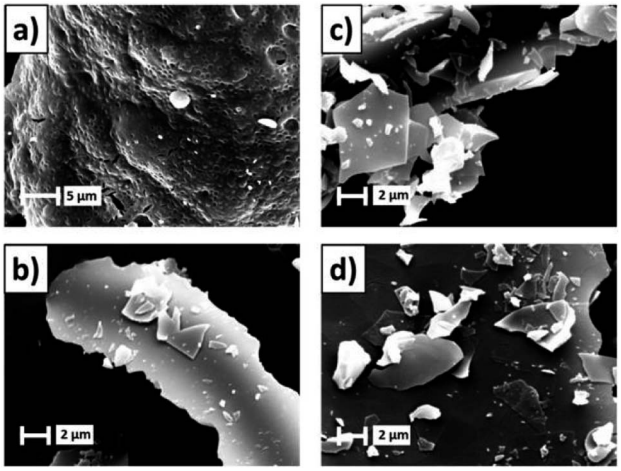

Fig. 7 The SEM images of the aluminas: (a) non-calcined; (b–d) calcined at 550, 750, 950 °C [reprinted with permission from ref. 38. Copyright 2021 Elsevier].

Maziviero *et al.* group successfully synthesized Al_2O_3 powders with high specific surface area (>200 m^2 g^{-1}) at microwave power of 450 W and lower fuel content. In addition, Fig. 7 shows the morphologies of the samples. The micrographs revealed powders with plate-like aggregates with irregular sizes.[38] Tamizhdurai *et al.* group successfully synthesized CeO_2 powders at microwave power of 750 W.[39] Microwave induced solution combustion method can rapidly and efficiently prepare different types of nano single metal oxides. The comprehensive properties of single metal oxide nanomaterials can be improved by process control.

3.2 Composite metal oxide nanomaterials

Composite metal oxides nanomaterials have a wide range of applications. Many methods have been derived for the preparation of composite metal oxide nanomaterials. The methods mainly include the sol–gel method,[40] microemulsion method,[41] co-precipitation method,[42] hydrothermal method,[43] and microwave-induced solution combustion method, *etc.* Among them, the microwave-induced solution combustion synthesis method is a green and efficient method and its simple operation, uniform heating, short heating time, and small particle size of products.

Therefore, the method is widely used for the preparation of the composite metal oxide nanomaterials. Table 2 lists some relevant reports on the synthesis of composite metal oxide nanomaterials by microwave-induced solution combustion.

The composite metal oxide nanomaterials prepared by microwave-induced solution combustion method have nanoscale microscopic size as well as high crystallinity. de Andrade *et al.* group successfully synthesized $MnFe_2O_4$ nanoparticles. The results of X-ray diffraction spectra showed that the synthesized material was the cubic phase of $MnFe_2O_4$ (JCPDS 73-1964). Fig. 8 shows that the formed $MnFe_2O_4$ nanoparticles were irregularly agglomerated in shape. The catalytic degradation of the malachite green (MG) cationic dye was investigated using a mixture of H_2O_2 and $MnFe_2O_4$ nanoparticles. The

Table 2 Microwave induced solution combustion synthesis composite metal oxide nanomaterials

Synthetic materials	Raw materials	Material characteristics	Particle/ crystallite size (nm)	Applications
$MnFe_2O_4$	$Mn(NO_3)_2 \cdot 4H_2O$ $Fe(NO_3)_3 \cdot 9H_2O$ $C_6H_8O_7$	Small particle size High crystallinity	7–40	Catalyst[44]
$CoFe_2O_4$	$Co(NO_3)_2 \cdot 6H_2O$ $Fe(NO_3)_3 \cdot 9H_2O$ $CO(NH_2)_2/C_2H_5NO_2/C_6H_8O_7$	—	—	Photocatalysis[45]
$NiFe_2O_4$	$Ni(NO_3)_2 \cdot 6H_2O$ $Fe(NO_3)_3 \cdot 9H_2O$ Plant extract	Small particle size High crystallinity High purity	50–70	Catalyst[51]
$BiFeO_3$	$Bi(NO_3)_3 \cdot 5H_2O$ $Fe(NO_3)_3 \cdot 9H_2O$ $C_6H_8O_7$	Good electrochemical properties High crystallinity	50–90	Catalyst[52]
Y_2O_3–MgO	$Mg(NO_3)_2 \cdot 6H_2O$ $Y(NO_3)_3 \cdot 6H_2O$ $C_6H_8O_7$	Small particle size High thermal stability	19	Transparent ceramic[53]
$ZnAl_2O_4$	$Zn(NO_3)_2 \cdot 4H_2O$ $Al(NO_3)_3 \cdot 9H_2O$ glycine/ethylene glycol/acetic acid	High surface area	—	Catalyst carrier[54]
$ZnFe_2O_4$	$Zn(NO_3)_2 \cdot 4H_2O$ $Fe(NO_3)_3 \cdot 9H_2O$ Plant extract solution	—	37/74	Solar cells[55]
Li_4SiO_4	$Si(OC_2H_5)_4$ $LiNO_3$ $C_6H_8O_7$	Small particle size High purity Favourable sinterability	25	Ceramic tritium breeders[56]

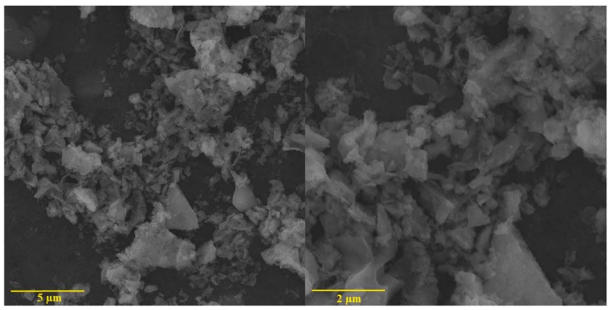

Fig. 8 The SEM image of $MnFe_2O_4$ nanoparticles [reprinted with permission from ref. 44. Copyright 2021 Elsevier].

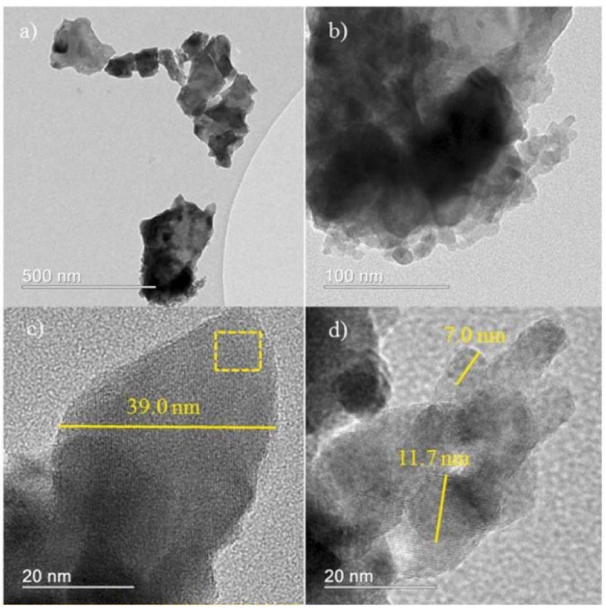

Fig. 9 High-resolution transmission electron microscopy (HRTEM) images (a–d) [reprinted with permission from ref. 44. Copyright 2021 Elsevier].

results suggested that the dye was completely decomposed after 60 min forming colourless products. In Fig. 9, Fig. 9(a) and (b) shows HRTEM images of $MnFe_2O_4$ nanoparticles. High-resolution transmission electron microscopy was used to better estimate the size of the formed particles. Their high magnification TEM images in Fig. 9(c) and (d) shows that the material consists of nanoparticles in the range of 7–40 nm.[44]

Microwave-induced solution combustion synthesis can be applied as a simple and effective synthesis method to improve the catalytic properties of spinel ferrite structured nanoparticles. Karakas *et al.* group successfully synthesized $CoFe_2O_4$ nanoparticles with thermally and chemically stable structures. By further investigating the effects of fuel type on the photocatalytic properties of the synthesized nanoparticles. The results showed that the dye was almost completely removed from the solution when the samples were prepared using citric acid. In addition, the removal efficiencies of the samples prepared with urea and glycine were 99% and 96%, respectively. Therefore, the improvement of the catalytic activity of cobalt ferrite nanoparticles can be achieved by adjusting the type of fuel.[45]

Compared with the conventional combustion method, the composite metal oxide nanomaterials synthesized by microwave-induced combustion have better microstructure and properties. Javadi *et al.* group successfully synthesized Cobalt ferrite ($CoFe_2O_4$) nanoparticles by conventional and microwave heating techniques. The results showed that the spherical $CoFe_2O_4$ nanoparticles synthesized by microwave heating are larger and have a higher saturation magnetization intensity compared to conventional heating.[46] Haghi *et al.* group successfully prepared $LiFePO_4$ powders using CTAB as fuel by conventional and microwave-assisted solution combustion methods. Compared with the conventional heating method, the $LiFePO_4$ powder synthesized by microwave heating has higher crystallinity, larger particle size and smaller specific surface area. In addition, the $LiFePO_4$ powders prepared by microwave heating method exhibited higher electrical conductivity due to lower electrode resistance.[47] Ragupathi *et al.* group successfully prepared nickel aluminate ($NiAl_2O_4$) using Opuntia dilenii haw as plant extract by conventional and microwave-assisted solution combustion methods. They found that the $NiAl_2O_4$ prepared by microwave combustion method is uniform in size and well-defined shape with crystallinity. The $NiAl_2O_4$ prepared by microwave combustion method was found to possess a higher specific surface area and smaller grain size than the $NiAl_2O_4$ synthesized by conventional combustion method.[48] Ajamein *et al.* group successfully synthesized Cobalt CuO–ZnO–Al_2O_3 nanocatalyst using ethylene glycol as fuel in the microwave oven and the conventional furnace. The results showed that the CuO prepared by the MCM method exhibited smaller particles, higher surface area and better crystallinity.[49] Kombaiah *et al.* group successfully prepared nanocrystalline $ZnFe_2O_4$ samples using Hibiscus rosa-sinensis plant extract as fuel by conventional and microwave-assisted solution combustion methods. The results showed that the $ZnFe_2O_4$ nanoparticles prepared by microwave-assisted combustion exhibited higher specific surface area and smaller grain size than the $ZnFe_2O_4$ nanoparticles prepared by conventional combustion.[50] In addition, Kombaiah *et al.* group successfully synthesized $NiFe_2O_4$ using plant extract as a fuel. Nickel nitrate and ferric nitrate was mixed in a molar ratio of 1 : 2 in a mortar pestle. Then the samples and plant extracts were dissolved double distilled water and stirred into a homogeneous clear solution. Finally, the solution will be ignited in a muffle and microwave oven to form $NiFe_2O_4$ powder. The results of XRD showed the synthesis of $NiFe_2O_4$ in a single crystalline phase with an average crystallite size of 50–70 nm. The particle sizes of the synthesized $NiFe_2O_4$ nanoparticles was observed using scanning electron microscopy (SEM). The $NiFe_2O_4$ nanoparticles with particle sizes in the range of 100–200 nm were synthesized by conventional combustion. However, the size of $NiFe_2O_4$ nanoparticles synthesized by microwave combustion was between 50–100 nm. Fig. 10 shows that the SEM image of $NiFe_2O_4$ synthesized by conventional solution combustion and microwave induced solution combustion. In addition, the

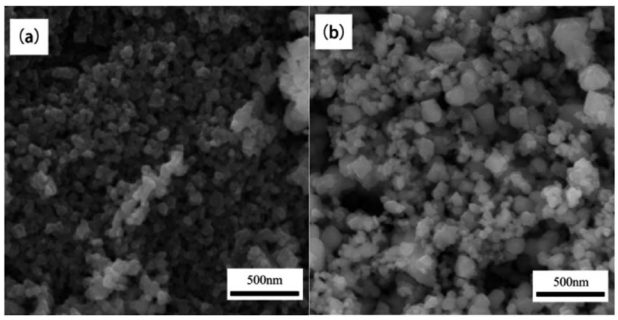

Fig. 10 The SEM image of $NiFe_2O_4$ nanoparticles: (a) conventional solution combustion synthesis, (b) microwave induced solution combustion synthesis [reprinted with permission from ref. 51. Copyright 2019 Elsevier].

catalytic reduction ability of $NiFe_2O_4$ nanoparticles for different dyes such as Rhodamine-B (RhB), Methylene blue (MB), Rose Bengal (RB), and Congo red (CR) was investigated. The results showed that the $NiFe_2O_4$ nanoparticles can be used as high potential catalyst for the reduction of organic dyes in wastewater treatment applications.[51]

Moradi *et al.* group successfully prepared $BiFeO_3$ and $BiFeO_3$ (CTAB/PVA/PEG) nanocomposites by a one-step green combustion synthesis. Hexadecyl trimethyl ammonium bromide (CTAB), polyvinyl alcohol (PVA), and polyethylene glycol (PEG-6000) are used as surfactants. The effect of surfactants on the catalytic performance of bismuth ferrate was investigated. The results showed that $BiFeO_3$-CTAB nano composites exhibited the highest degradation rate of methyl orange dye contamination, and the degradation rate could be increased up to 97% in aqueous solution.[52] Mathew *et al.* group prepared Y_2O_3–MgO nanocomposites by one-step microwave sintering. The XRD analysis results showed the presence of ultrafine nanostructured Y_2O_3 and MgO cubic phases with an average microcrystal size of about 19 nm. Fig. 11(a) shows the TEM image of Y_2O_3–MgO nanocomposite. TEM images exhibited that the crystal size ranges from 12 nm to 24 nm. Fig. 11(b) shows the different crystal planes of Y_2O_3–MgO nanocomposites. From the clearly visible grains, the grain size is calculated to be 15.6 nm, corresponding to the (222) plane of cubic crystal structure of Yttrium.[53]

Talati *et al.* group successfully synthesized $ZnAl_2O_4$ nanoparticles using $Zn(NO_3)_2 \cdot 4H_2O$ and $Al(NO_3)_3 \cdot 9H_2O$ as oxidants and glycine (Gly), ethylene glycol (EG), and acetic acid (AA) as reducing agents by the one-step microwave combustion (MW) method and muffle-furnace combustion (MF). In the process of synthesis, $Zn(NO_3)_2 \cdot 4H_2O$ and $Al(NO_3)_3 \cdot 9H_2O$ in Zn/Al molar ratio of 1/2 were dissolved into deionized water. Then the fuel

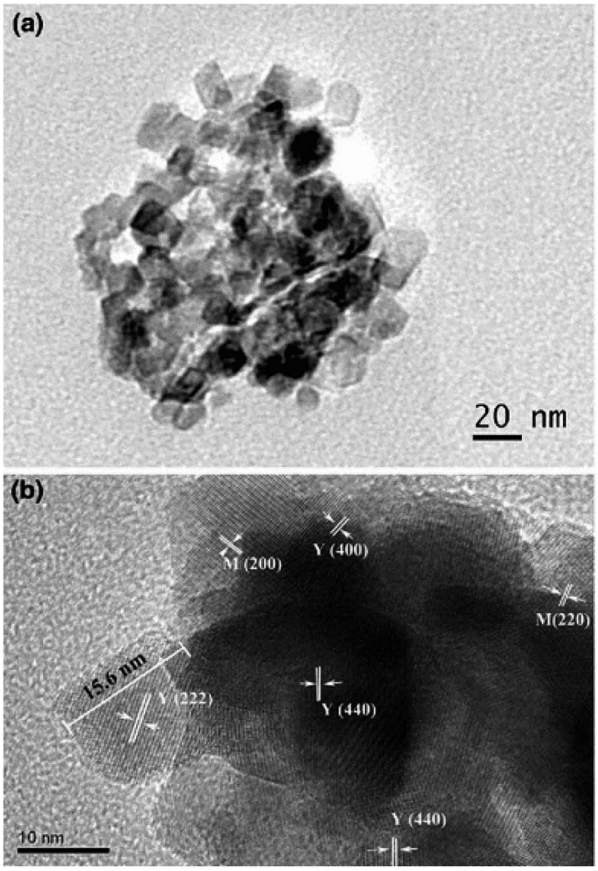

Fig. 11 (a) TEM image of as-prepared nano Y_2O_3–MgO nanocomposite. (b) HRTEM image of different crystallographic planes [reprinted with permission from ref. 53. Copyright 2017 Indian Academy of Science].

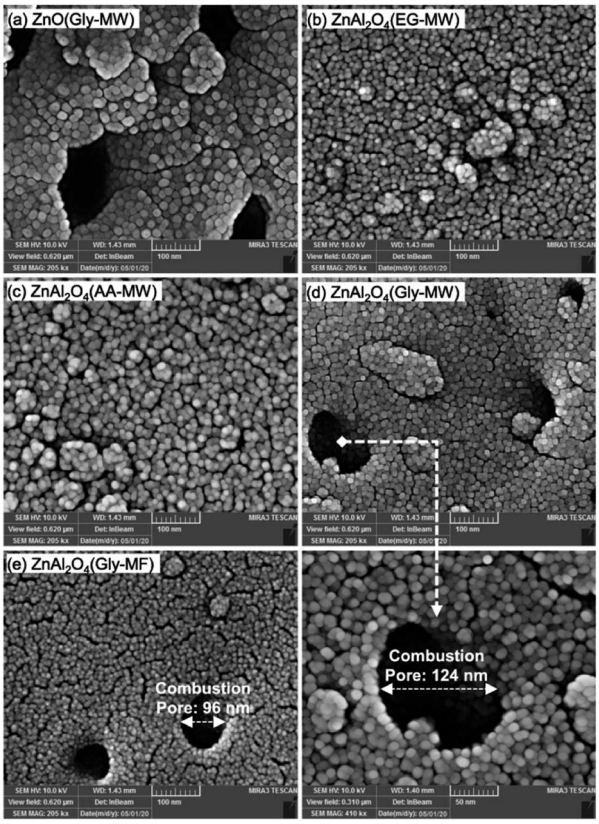

Fig. 12 The FESEM image of Zn-spinel nanophotocatalysts: (a) ZnO(Gly-MW), (b) $ZnAl_2O_4$(EG-MW), (c) $ZnAl_2O_4$(AA-MW), (d) $ZnAl_2O_4$(Gly-MW), (e) $ZnAl_2O_4$(Gly-MF) [reprinted with permission from ref. 54. Copyright 2022 Elsevier].

was added into the solution at the stoichiometric ratio and vigorously stirred. In the next stage, the mixture temperature was raised to 60 °C and continue stirring until a transparent gel was formed. Finally, the generated transparent gel was put into a microwave oven at 950 W for 2 min to synthesize $ZnAl_2O_4$ nanoparticles. As shown in Fig. 12(a), the surface morphology of the ZnO nanophotocatalyst synthesized with glycine consists of spherical nanoparticles with large pores. In Fig. 12(b) and (c), the surface morphology of the $ZnAl_2O_4$ nanophotocatalyst synthesized by ethylene glycol and acetic acid consists of continuous spherical agglomerates with low porosity. In contrast, the synthesized Zn-spinel samples with glycine (Fig. 12(d) and (e)) have porous structures with big combustion pores.[54] Compared with the conventional solution combustion method, the microwave-induced solution combustion method is a more promising simple, efficient and energy saving material preparation method, which produces composite metal oxide nanomaterials with better stability and higher purity. Due to its unique heating mechanism, the process of microwave-induced solution combustion can reduce the production of impurity phases.

Kombaiah *et al.* group successfully prepared $ZnFe_2O_4$ nanomaterials using iron nitrate and zinc nitrate as oxidants and plant extracts as fuel (reducing agent) by conventional solution combustion and microwave-induced solution combustion methods. In addition, they studied the effect of two different heating methods on the performance of the synthesized materials. The results showed that the maximum conversion rate of solar cells composed of $ZnFe_2O_4$ prepared by microwave-induced combustion method could reach 0.22%, which is higher than the conversion efficiency of samples prepared by conventional combustion method. The particle sizes of the synthesized $NiFe_2O_4$ nanoparticles was observed using scanning electron microscopy (SEM). The $ZnFe_2O_4$ nanoparticles with particle sizes in the range of 5–15 nm were synthesized by conventional combustion. However, the size of $ZnFe_2O_4$ nanoparticles synthesized by microwave combustion was between 30-50 nm.[55] Zhou *et al.* group synthesized lithium orthosilicate (Li_4SiO_4) by microwave induced solution combustion synthesis using tetraethyl orthosilicate ($Si(OC_2H_5)_4$) and lithium nitrate ($LiNO_3$) as oxidants and citric acid as fuel. The research found that the content of Li_2SiO_3 in the product could be effectively reduced by regulating the microwave power and the ratio of fuel to oxide. When the microwave power output is 1100 W and the φ value is 0.75, the Li_2SiO_3 content can be minimized. In addition, the thermal analysis revealed that the relative density of the ceramic embryos after calcination at the sintering temperature of 1373 K was as high as 96%, which is an ideal material for tritium-augmented ceramics.[56] Sundararajan *et al.* group synthesized $NiFe_2O_4$ and $ZnFe_2O_4$ nanoparticles with average grain size ranging from 16 to 20 nm using microwave induced solution combustion method.[57]

Mahmoud *et al.* group successfully prepared $NiFe_2O_4$ using metal nitrates and urea as starting materials by a microwave-induced combustion method and investigated the effect of fuel-to-oxidizer ratio on their particle size during the combustion process. The results showed that the particle size can be systematically controlled by simply changing the urea/metal nitrate ratio. When the urea is relatively low, the sample is less crystalline.[58]

3.3 Ion doping metal oxide nanomaterials

The microwave-induced solution combustion synthesis method has also been mostly used to prepare ion-doped metal oxide nanomaterials. This method is not only simple, low-cost, and efficient, but also can improve the microstructure and properties of ion-doped nano-metal oxides. Zhao *et al.* group successfully prepared neodymium aluminum lutetium-doped garnet (LuAG: Nd) phosphor materials with particle sizes ranging from 100 to 130 nm using microwave induced solution combustion synthesis. Fig. 13 shows the microscopic morphology of the synthesized LuAG: Nd at different calcination temperatures. The results showed that the microwave induced solution combustion synthesized LuAG: Nd grains as regular spherical grains when the calcination temperature was 900 °C.

In addition, the fluorescence emission spectra of LuAG: Nd powders with different Nd^{3+} doping concentrations were detected. The results showed that the highest emission peak intensity of fluorescence spectrum can be observed at 1064 nm for LuAG: Nd powders when the Nd^{3+} doping concentration is 5 mol%. The results indicated that the LuAG: Nd phosphor synthesized by microwave-induced solution combustion is a promising optical material.[59]

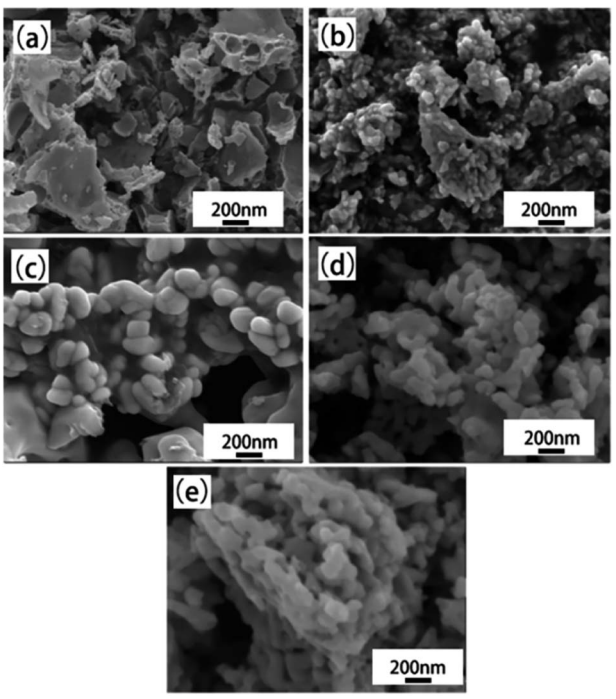

Fig. 13 The SEM images of $Lu_{2.85}Nd_{0.15}Al_5O_{12}$ powders prepared with different temperatures: (a) 800 °C, (b) 850 °C, (c) 900 °C, (d) 950 °C, (e) 1000 °C [reprinted with permission from ref. 59. Copyright 2020 Elsevier].

Compared with the conventional combustion method, the ion-doped metal oxide nanomaterials synthesized by microwave-induced combustion have better microstructure and properties. Chen *et al.* group successfully synthesized pure and well-crystallized $BaMgAl_{10}O_{17}$: Eu^{2+} (BAM) nanoscale blue phosphors by adopting a feasible microwave-induced solution combustion synthesis (MISCS) method. By studying the BAM synthesized by traditional solution combustion and microwave solution combustion, the results showed that the BAM phosphor synthesized by microwave solution combustion exhibited good spherical morphology, good crystallinity, and strong blue light emission ability under vacuum ultraviolet (VUV) light excitation. In Fig. 14, The TEM and high-resolution TEM (HRTEM) images of BAM shows the lattice fringes with a lattice spacing of 0.486 nm, corresponding to the (0 0 1) plane of β-alumina-structured BAM. It is known that the dipole molecules (H_2O) are constantly rotating in the presence of microwave radiation, which generates heat in the microwave oven. Therefore, the reactions are uniformly heated in the microwave oven compared to the reactions in conventional heating systems,[60] which helps to increase the reaction rate. The main advantage of the introduction of microwave into the reaction system is the extremely rapid crystallization kinetics,[61] so that smaller particle sizes and well crystallized particles can be imagined.[62]

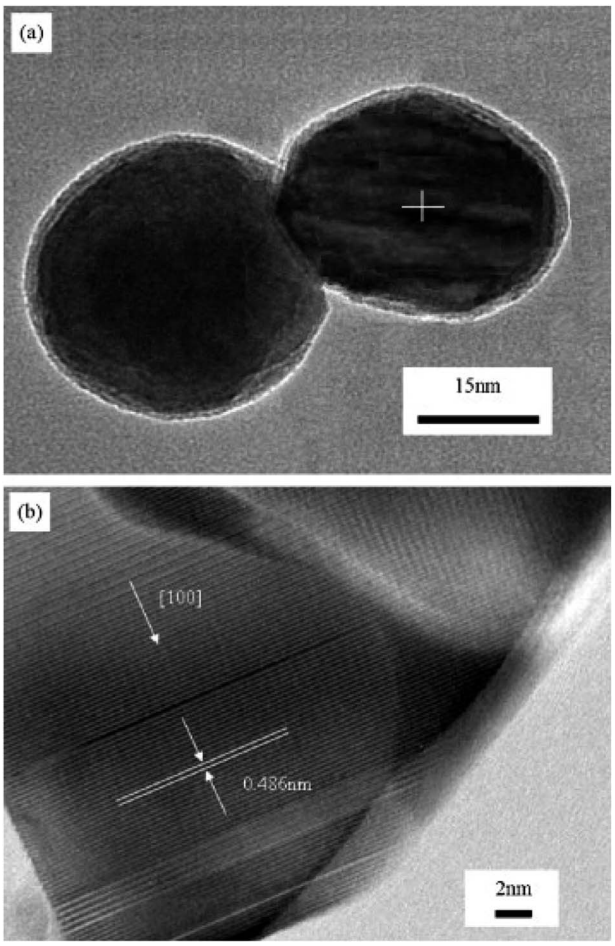

Fig. 14 (a) TEM image of BAM nanoparticle; (b) high-resolution TEM image of the BAM in Fig. 2(a) [reprinted with permission from ref. 62. Copyright 2009 Elsevier].

The ion-doped metal oxide nanomaterials prepared by microwave-induced solution combustion synthesis are characterized by small particle size, large specific surface area, and the preparation process is simple. Medeiros *et al.* group prepared nickel based catalysts with alumina (Al_2O_3) as the carrier by microwave-induced solution combustion synthesis using aluminum nitrate nonahydrate and nickel nitrate nonahydrate as oxidants and urea as reducing agent. In addition, the effect of the fuel-to-oxidizer ratio on the catalytic performance of the prepared products was investigated. The results showed that the nickel-based catalysts prepared with alumina (Al_2O_3) as the carrier at low fuel ratio (fuel-to-oxidizer ratio less than 50% of the stoichiometric ratio) have a high reduction, high specific surface area (265 m^2 g^{-1}) and small size (~15 nm). These properties make the catalytic performance of nickel-based catalysts improved.[63] Baskar *et al.* group synthesized strontium ion-doped cubic crystalline magnesium ferrite using arginine as a fuel after reacting at 700 W microwave power for 15 min. The average particle size was calculated from 24.11 to 33.10 nm by the Debay–Scherrer formula. The presence of Sr, Mg, Fe and O was confirmed by EDX studies.[64]

Palan *et al.* group prepared $BaLaB_9O_{16}$ doped and co-doped with Eu^{3+} and Tb^{3+} by microwave induced solution combustion. The research found that microwave assisted heating resulted in better sintering properties of the products.[65] Ansari *et al.* group dissolved zinc nitrate, dopant nitrate (Fe, Al, Cr, and Li), and glucose fuel in distilled water in accordance with the stoichiometric ratio, heated in a microwave oven for 2–3 min, and then placed in a preheated furnace at 500 °C. After heating in the furnace for 10 min, $Zn_{0.94}M_{0.06-x}Li_xO$ (M: Fe^{3+}, Al^{3+}, Gr^{3+}) nanoparticles were synthesized. In addition, the effect of different ion doping on the photocatalytic efficiency of ZnO catalysts in the degradation of rhodamine B dye was investigated. The results showed that the photodegradation efficiencies of CZO (6 mol% Gr^{3+}-doped ZnO), AZO (6 mol% Al^{3+}-doped ZnO), and L3AZO (1.5 mol% Li^{+}-ion co-doped AZO) catalysts were higher compared with the photodegradation efficiencies of ZnO catalysts (89%).[66] Kanithan *et al.* group used nickel nitrate, iron nitrate, and magnesium nitrate as oxidants and arginine as fuel to synthesize undoped nickel ferrite spinel ($NiFe_2O_4$) and magnesium doped nickel ferrite spinel ($Ni_{1-x}Mg_xFe_2O_4$). The undoped $NiFe_2O_4$ has a single-phase cubic spinel structure with an average crystallite size between 20 and 35 nm, while the magnesium-doped $NiFe_2O_4$ also has a cubic spinel structure. In addition, doping of magnesium ions will induce secondary crystallization of the α-Fe_2O_3 phase. Fig. 15 shows the SEM images of undoped Mg^{2+} ($x = 0$) and doped Mg^{2+} ($x = 0.1$).[67] Dhiwahar *et al.* group successfully prepared $Cu_{1-x}Co_xFe_2O_4$ with different cobalt contents by microwave-induced solution combustion method. In addition, the effect of doping with or without cobalt ions on the degradation of rhodamine B by copper ferrites under visible light ($k > 420$ nm) irradiation was investigated. The results showed that the degradation effect increased with the content of doped cobalt ions.[68]

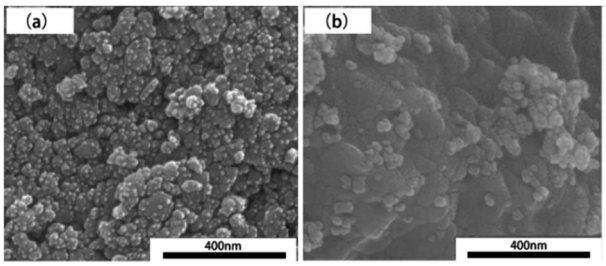

Fig. 15 The SEM image of $Ni_{1-x}Mg_xFe_2O_4$ nanoparticles: (a) undoped magnesium ion ($x = 0$), (b) doped magnesium ion ($x = 0.1$) [reprinted with permission from ref. 67. Copyright 2022, Elsevier.

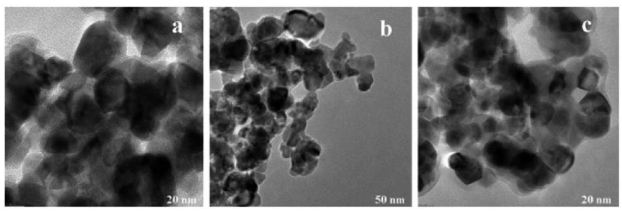

Fig. 16 TEM micrographs of $Zn_xNi_{1-x}Fe_2O_4$ nanoparticles where x is (a) 0.0, (b) 0.2, and (c) 0.7, synthesized by microwave assisted combustion method [reprinted with permission from ref. 69. Copyright 2009 Elsevier].

Sertkol *et al.* group successfully synthesized $Zn_xNi_{1-x}Fe_2O_4$ using metal nitrates and urea as starting materials by microwave-assisted combustion method. In Fig. 16, the TEM analysis results shows the presence of necked near-spherical particles with an average size of ~20 nm.[69] Freitas *et al.* group successfully synthesized nanocrystalline $Ni_xCo_{1-x}Fe_2O_4$ from nitrate precursors, using urea as fuel. The TEM analysis results showed the presence of Near-spherical and necked particles with an average crystallite size of 30 to 50 nm.[70] Chamani *et al.* group successfully prepared Co_xNi_{1-x}ferrite nanoparticles with varying compositions by microwave auto-combustion method. In Fig. 17, the high-resolution TEM (HRTEM) images of $Co_{0.9}$-$Ni_{0.1}$ferrite shows the lattice fringes with a lattice spacing of 0.496 nm, corresponding to the (111) of CoFerrite.[71]

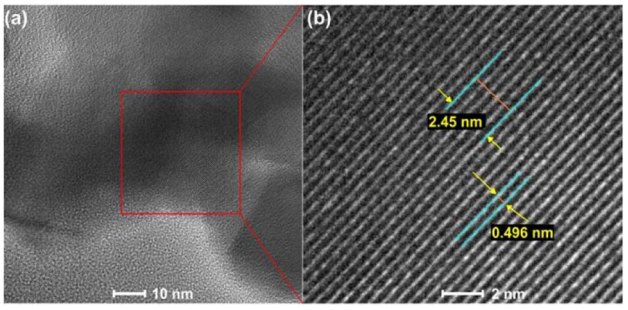

Fig. 17 (a, b) HRTEM images of $Co_{0.9}Ni_{0.1}$Ferrite [reprinted with permission from ref. 71. Copyright 2021 American Chemical Society].

4 Influence of process parameters related to microwave-induced solution combustion synthesis of nanomaterials

In the process of microwave-induced solution combustion synthesis of nanomaterials, a series of parameters such as microwave power, the dosage ratio of oxidant to fuel, the type of fuel, and the pH value of the precursor solution will have certain effects on the microstructure and properties of the products.

4.1 Influence of fuel type

The presence of fuel plays a crucial role in the synthesis of nanomaterials by microwave-induced solution combustion. During the combustion reaction, the fuel not only acts as a reducing agent but also has good complexation. In addition, the fuel can form a gel network with metal ions to prevent early precipitation of metal ions, maintain the compositional homogeneity between all components, and contribute to the formation of strong coordination bonds.[72] Therefore, the fuel type has a great influence on the microstructure of the final oxidized material.

Azizi *et al.* group investigated the microstructural changes of the ZnO nanoparticles using zinc nitrate as an oxidant and the fruits, seeds, and pulp of citrus as fuel. The results revealed that the average particle size of the synthesized ZnO nanoparticles ranged from 27 to 85 nm. The shapes of the ZnO particles synthesized with fruits, seeds, and pulp were a flower-like, hexagonal, and blocky nanostructures, respectively.[36] Mahu *et al.* group used urea, citric acid, and maleic acid as fuels and successfully prepared $CoFe_2O_4$ and $NiFe_2O_4$ nanoparticles. Among the three different fuels, the $CoFe_2O_4$ and $NiFe_2O_4$ nanoparticle samples prepared with urea as fuel had the smallest grain size and the highest specific surface area.[73] Karakas *et al.* group synthesized $CoFe_2O_4$ powders by combustion using $Co(NO_3)_2 \cdot 6H_2O$ and $Fe(NO_3)_3 \cdot 9H_2O$ as oxidants and urea, glycine, and citric acid as fuels. The effect of the type of fuel added on the structure and morphology of the synthesized $CoFe_2O_4$ nanoparticles was investigated. The results showed that the samples synthesized with urea had the smallest particle size. The samples prepared with glycine had more uniform morphology and proper shape, but their average particle size was observed to be larger than the other samples.[45]

Rasouli *et al.* group successfully prepared Europium oxide doped with zinc oxide using microwave-assisted combustion method. In addition, the effect of different types of fuels on the structural morphology of the synthesized nanoparticles was investigated. The results showed that the morphology of the samples shifted from nanosphere to sponge-like when the fuel mixture composition changed from citric acid to glycine.[74] Khort *et al.* group produced metallic cobalt nanoparticles by microwave-assisted combustion and investigated the effects of different types of fuels (urea, citric acid, glycine and hexamethylenetetramine) on the combustion process and solid product properties. When hexamethylenetetramine was used as a fuel, the results showed that metallic Co nanoparticles with a wide size distribution (~5–40 nm) could be synthesized by one-step solution combustion under normal air atmosphere.[75]

4.2 Influence of the dosage ratio of oxidant to fuel

During the reaction of microwave-induced solution combustion synthesis, the different dosage ratios of oxidant to fuel can have a great influence on the microstructure and properties of the products. Luiz *et al.* group prepared niobium pentoxide (Nb_2O_5) powder by this method and investigated the effect of the dosage of ammonium niobium oxalate and urea on the microstructure of the products. When the dosage ratio of oxidant to fuel was the stoichiometric ratio, the resulting Nb_2O_5 had the largest particle size, while excess of fuel or excess of oxidant will give smaller particle size of Nb_2O_5. This is mainly because the amount of oxidant and fuel can change the temperature of the reaction process, which affects the size of the resulting particles. Excessive amounts of both oxidant and fuel lowered the reaction synthesis temperature and slowed down the growth of the particles.[35] Nayebzadeh *et al.* group used the microwave combustion method to prepare zirconia-alumina nanocatalysts and investigated the effect of fuel-to-oxidizer ratio (F/O) on their structural and chemical properties during the combustion process. The results showed that when the fuel-to-oxidizer ratio increased from 0.5 to 1.0, the combustion reaction temperature and time increased, leading to the formation of ZrO and α-Al_2O_3. The crystal size of zirconia-alumina nanocatalysts increased when the fuel-to-oxidizer ratio was increased from 1 to 1.5.[76]

Derakhshani *et al.* group prepared hierarchical porous $Ni_{0.5}Zn_{0.5}Fe_2O_4$ ferrite powder using metal nitrate as oxidant and glycine as fuel. By investigating the effect of fuel content on the composition of the synthesized material, the results showed that the pure NiZn ferrite powder was directly crystallized at lower fuel content, and about 2 wt% intermetallic $FeNi_3$ phase appeared at fuel to total metal nitrates molar ratio of 2.[77] Frikha *et al.* group prepared three binary metal oxide catalysts containing Ni, Cu, and Co oxides using microwave-assisted solution combustion method. The results showed that the performance of the catalysts prepared by microwave-assisted solution combustion can be improved by controlling the reactant stoichiometric ratio (RV/OV). Catalysts with the best structural properties and the best catalytic activity can be prepared at the stoichiometric balance (RO/RV = 1). On the contrary, when the RV/OV ratio of the catalysts was non-stoichiometric balance, the combustion reactions were not controlled, thus resulting to poor structural properties of the catalysts.[78]

4.3 The pH of the precursor solution

The pH of the precursor solution also plays a crucial role in the microwave-induced solution combustion synthesis of nanomaterials, mainly affecting the intensity of the combustion process and the structural morphology of the final oxidized material.[72] Radpour *et al.* group formulated precursor solutions using $Al(NO_3)_3 \cdot 9H_2O$ as an oxidant and $C_6H_8O_7$ as fuel. Then ammonia was added to adjust the pH value of the solution to 2, 7, and 9. The iron oxide nanopowders were synthesized at different pH conditions. The average particle sizes of the synthesized Fe_3O_4 were 10 nm, 25 nm, and 27 nm when the pH values were 2, 7, and 9, respectively. In addition, when the pH = 2, the iron oxide (Fe_3O_4) was generated, and when the pH = 7 or the pH = 9, in addition to Fe_3O_4, the FeO phase was also generated.[79] Araichimani *et al.* group prepared Fe_3O_4-modified SiO_2 nanostructures by microwave-induced combustion method using rice husk as the silicon source. The effect of pH of the precursor solution on the ability of the synthesized samples to adsorb Hg^{2+} was also investigated. The results showed that increasing the pH of the precursor solution could increase the removal rate of Hg^{2+}. The removal rate of Hg^{2+} reached the maximum when pH = 6. This is mainly due to the fact that only a small amount of mercury ions (Hg^{2+}) are adsorbed on the surface of the prepared samples at lower pH values. Besides, the amount of hydrogen ions (H^+) decreased significantly with increasing pH, resulting in enhanced adsorption of Hg^{2+} on the prepared samples at pH = 6.[80]

4.4 Microwave power

In the process of microwave-induced solution combustion synthesis, different microwave powers affect the phase composition and microstructure of the products. Zhou *et al.* group prepared Li_4SiO_4 nanoparticles by microwave-induced solution combustion synthesis and investigated the effect of different microwave powers on the composition of the product phases by adjusting the microwave power to 700 W, 900 W, 1100 W, and 1300 W. The results showed that the Li_4SiO_4 powders produced by microwave-induced solution combustion synthesis at four different microwave powers contained a small amount of Li_2SiO_3. When the microwave output power was 1100 W, the content of Li_2SiO_3 decreased to 5%, which improved the purity of the products.[56] Yathisha *et al.* group synthesized prismatic zinc oxide (ZnO) nanostructures by microwave combustion method using zinc nitrate as precursor and ethylene glycol as solvent at different microwave powers (160, 320, 480, 640 and 800 W). XRD and FE-SEM results confirmed the dependence of grain size and growth of ZnO nanostructures on microwave heating power.[81]

Hashemzehi *et al.* group successfully synthesized zinc-aluminum spinel as well as copper-aluminum spinel by microwave induced solution combustion method. The effect of microwave power on the microstructure of the synthesized zinc-aluminum spinel as well as copper aluminum spinel was also investigated to obtain zinc/copper-aluminum spinel with small grain size and less agglomerated particles. The experimental results showed that the higher microwave power is beneficial to the improvement of the morphology and structure of zinc/copper aluminum spinel nanoparticles. The growth of pore diameter was resulted by increasing microwave power.[82]

5 Conclusions and prospect

Currently, the microwave-induced solution combustion method is widely used in the synthesis and preparation of nanomaterials. Compared with the traditional heating method, the advantages of the microwave-induced solution combustion method are reflected in the uniform heating of the reaction

mixture, high selectivity, clean products, good reproducibility, and energy saving.

In addition, the method can significantly shorten the reaction time of the reactants and effectively reduce the generation of by-products during the reaction process, thus contributing to energy conservation and rapid preparation of the target products. Microwave synthesis technology has contributed greatly to the preparation of nanomaterials of various sizes and well-defined structures with the premise of using liquid substances as the reaction medium. Although the microwave-induced solution combustion synthesis method has a series of advantages such as high efficiency and energy saving, there are still some difficulties to be solved:

(1) Regarding the mechanism of microwave heating, some people think that the heat generated by microwave heating is due to depolarization, while others think that the heat generated by microwave heating is caused by Ionic conductance. The mechanism of microwave heating can not be clearly explained at present. Therefore, it is necessary to further understand the nature of the reaction mechanism in the future.

(2) The controlled preparation of nanomaterials with different structures, morphologies, and properties can be achieved by regulating the parameter settings of microwave heating methods.

(3) The reaction space of microwave heating equipment is relatively small, which leads to the high cost of mass production. Therefore, further optimization of the microwave heating equipment is required.

(4) The method of microwave-induced solution combustion synthesis does not have the conditions for continuous production. Therefore, it is possible to provide a possibility for continuous production of microwave-induced solution combustion synthesis of nanopowders by improving the synergy between the equipment.

Conflicts of interest

There are no conflicts to declare.

Acknowledgements

This work was financially supported by the National Natural Science Foundation of China (No. 51472220, No. 51872265), and Collaborative Innovation Major Special Project of Zhengzhou (No. 20XTZX12025).

References

1 H. Gleiter, *Acta. Metall. Sin.*, 1997, **33**, 165–174.
2 K. Shehzad, Y. Xu, C. Gao and X. Duan, *Chem. Soc. Rev.*, 2016, **45**, 5541–5588.
3 Y. Yao, Y. Wei and S. Chen, *Surf. Sci.*, 2015, **636**, 19–24.
4 L. Zhang, L. Yin, C. Wang, N. Lun, Y. Qi and D. Xiang, *J. Phys. Chem. C*, 2010, **114**, 9651–9658.
5 A. Verma and F. Stellacci, *Small*, 2010, **6**, 12–21.
6 N. V. Ilawe, M. Belen Oviedo and B. M. Wong, *J. Mater. Chem. C*, 2018, **6**, 5857–5864.
7 Y. R. Parauha, V. Sahu and S. J. Dhoble, *Mater. Sci. Eng., B*, 2021, **267**, 115054.
8 D. Wang and Y. Chang, *Nanomaterials*, 2022, **12**, 572.
9 D. P. Harris, C. Wan, Y. She, B. R. Beck, D. S. Forbes and B. M. Leonard, *Z. Naturforsch., B: J. Chem. Sci.*, 2021, **76**, 803–810.
10 R. Yu, F. Liu, H. Ren, J. Wu and X. Zhang, *Environ. Technol.*, 2018, **39**, 2162–2167.
11 Y. Chang, B. Liu, Z. Huang, Y. Liu, M. Liu and J. Liu, *Langmuir*, 2020, **36**, 1034–1042.
12 D. Shi, H. Yang and X. Xue, *Chin. J. Chem. Eng.*, 2020, **28**, 1474–1482.
13 T. Cai, G. Fang, X. Tian, J.-J. Yin, C. Chen and C. Ge, *ACS Nano*, 2019, **13**, 12694–12702.
14 L. Katsnelson and B. Kerbel, *Non-Ferrous Pyrometall.: Trace Met., Furn. Pract. Energy Effic., Proc. Int. Symp.*, 2012, **1**, 34–37.
15 L. Zhang, Z. Li, F. Zhen, L. Wang, Q. Zhang, R. Sun, F. A. Selim, C. Wong and H. Chen, *J. Mater. Sci.*, 2017, **52**, 8556–8567.
16 W. He, P. Song, B. Yu, Z. Fang and H. Wang, *Prog. Mater. Sci.*, 2020, **114**, 100687.
17 S. R. Jain, K. C. Adiga and V. R. Pai Verneker, *Combust. Flame*, 1981, **40**, 71–79.
18 D. Evecan, Ş. S. Kaplan, M. Ş. Sönmez, S. Yıldırım, M. Okutan, H. Deli-gçz and E. Zayim, *Microelectron. Eng.*, 2019, **215**, 110989.
19 D. Zheng, G. Wang, W. Huang, B. Wang, W. Ke, J. L. Logsdon, H. Wang, Z. Wang, W. Zhu, J. Yu, M. R. Wasielewski, M. G. Kanatzidis, T. J. Marks and A. Facchetti, *Adv. Funct. Mater.*, 2019, **29**, 1900265.
20 S. L. González-Cortés and F. E. Imbert, *Appl. Catal., A*, 2013, **452**, 117–131.
21 K. K. Banger, Y. Yamashita, K. Mori, R. L. Peterson, T. Leedham, J. Rick-ard and H. Sirringhaus, *Nat. Mater.*, 2011, **10**, 45–50.
22 Z. Shao, W. Zhou and Z. Zhu, *Prog. Mater. Sci.*, 2012, **57**, 804–874.
23 B. N. Rao and N. Satyanarayana, *ECS J. Solid State Sci. Technol.*, 2021, **10**, 103003.
24 G. A. Tompsett, W. C. Conner and K. S. Yngvesson, *ChemPhysChem*, 2006, **7**, 296–319.
25 Y. J. Zhu and F. Chen, *Chem. Rev.*, 2014, **114**, 6462–6555.
26 C. O. Kappe, *Angew. Chem., Int. Ed.*, 2004, **43**, 6250–6284.
27 D. V. Stass, J. R. Woodward, C. R. Timmel, P. J. Hore and K. A. McLauchlan, *Chem. Phys. Lett.*, 2000, **329**, 15–22.
28 M. J. Collins Jr, *Future Med. Chem.*, 2010, **2**, 151–155.
29 B. L. Hayes, *Microwave synthesis: Chemistry at the speed of light*, Cem Corporation, 2002.
30 C. O. Kappe, D. Dallinger and S. S. Murphree, *Strategies, Instruments, and Protocols*, Wiley-VCH, Weinheim, Germany, 2009.
31 P. Michael and D. áMingos, *Chem. Soc. Rev.*, 1991, **20**, 1–47.
32 T. Patra, J. Panda and T. R. Sahoo, *Mater. Today: Proc.*, 2021, **41**, 247–250.
33 G. T. Anand, S. J. Sundaram, K. Kanimozhi, R. Nithiyavathi and K. Kaviyarasu, *Mater. Today: Proc.*, 2021, **36**, 427–434.

34 B. Priyadarshini, T. Patra and T. R. Sahoo, *J. Magnesium Alloys*, 2021, **9**, 478–488.
35 T. M. Luiz, F. Nakagomi, R. A. Renzetti and G. O. Siqueira, *Process. Appl. Ceram.*, 2021, **15**, 128–135.
36 S. Azizi, R. Mohamad and M. M. Shahri, *Molecules*, 2017, **22**, 301.
37 M. Radpour, S. M. Masoudpanah and S. Alamolhoda, *Ceram. Int.*, 2017, **43**, 14756–14762.
38 F. V. Maziviero, R. L. B. A. Medeiros, D. M. A. Melo, H. P. Macedo, A. A. S. Oliveira and T. R. Araujo, *Mater. Chem. Phys.*, 2021, **264**, 124408.
39 P. Tamizhdurai, S. Sakthinathan, S.-M. Chen, K. Shanthi, S. Sivasanker and P. Sangeetha, *Sci. Rep.*, 2017, **7**, 1–13.
40 S. V. Bhandare, R. Kumar, A. V. Anupama, H. K. Choudhary, V. M. Jali and B. Sahoo, *J. Magn. Magn. Mater.*, 2017, **433**, 29–34.
41 A. Karimi, M. A. A. Sadatlu, B. Saberi, H. Shariatmadar and M. Ashjaee, *Adv. Powder Technol.*, 2015, **26**, 1529–1536.
42 T. Zhang, D. Gong, S. Lin and J. Yu, *Chem. Eng. J.*, 2022, **449**, 137830.
43 M. Srivastava, S. Chaubey and A. K. Ojha, *Mater. Chem. Phys.*, 2009, **118**, 174–180.
44 F. V. de Andrade, A. B. de Oliveira, G. O. Siqueira, M. M. Lage, M. R. de Freitas, G. M. de Lima and J. Nuncira, *J. Environ. Chem. Eng.*, 2021, **9**, 106232.
45 I. H. Karakas, *Ceram. Int.*, 2021, **47**, 5597–5609.
46 S. Javadi, S. M. Masoudpanah and A. Zakeri, *J. Sol-Gel Sci. Technol.*, 2016, **79**, 176–183.
47 Z. Haghi and S. M. Masoudpanah, *J. Sol-Gel Sci. Technol.*, 2019, **91**, 335–341.
48 C. Ragupathi, J. J. Vijaya and L. J. Kennedy, *J. Saudi Chem. Soc.*, 2017, **21**, 231–239.
49 H. Ajamein and M. Haghighi, *Energy Convers. Manage.*, 2016, **118**, 231–242.
50 K. Kombaiah, J. J. Vijaya, L. J. Kennedy and M. Bououdina, *Ceram. Int.*, 2016, **42**, 2741–2749.
51 K. Kombaiah, J. J. Vijaya, L. J. Kennedy and K. Kaviyarasu, *Mater. Chem. Phys.*, 2019, **221**, 11–28.
52 E. Moradi, H. Farajnejad Ghadi, M. Rabbani and R. Rahimi, *J. Mater. Sci.: Mater. Electron.*, 2021, **32**, 8237–8248.
53 C. T. Mathew, S. Solomon, J. Koshy and J. K. Thomas, *Biomater. Sci.*, 2017, **40**, 1171–1178.
54 A. Talati and M. Haghighi, *Sol. Energy*, 2022, **234**, 275–293.
55 K. Kombaiah, J. J. Vijaya, L. J. Kennedy and M. Bououdina, *Optik*, 2017, **129**, 57–68.
56 Q. Zhou, J. Zhou, W. Feng, L. Xue, H. Li, L. Guo and Y. Yan, *Ceram. Int.*, 2021, **47**, 22006–22015.
57 M. Sundararajan, M. Sukumar, C. S. Dash, A. Sutha, S. Suresh, M. Ubaidullah, A. M. Al-Enizi, M. K. Raza and D. Kumar, *Phys. Rev. B: Condens. Matter Mater. Phys.*, 2022, **644**, 414232.
58 M. H. Mahmoud, A. M. Elshahawy, S. A. Makhlouf and H. H. Hamdeh, *J. Magn. Magn. Mater.*, 2013, **343**, 21–26.
59 C. Zhao, J. Yu, Y. Zhang, H. Gong, B. Xie, X. Lin, M. Sheng, J. Mao and J. Jing, *Ceram. Int.*, 2020, **46**, 17891–17895.
60 R. A. KIMINAMI, M. R. Morelli, D. C. Folz and D. E. Clark, *Am. Ceram. Soc. Bull.*, 2000, **79**, 63–67.
61 W. W. Wang, *Mater. Chem. Phys.*, 2008, **108**, 227–231.
62 Z. Chen, Y. Yan, J. Liu, Y. Yin, H. Wen, J. Zhao and S. Li, *J. Alloys Compd.*, 2009, **473**, 13–16.
63 R. L. B. A. Medeiros, G. P. Figueredo, H. P. Macedo, A. A. S. Oliveira, R. C. Rabelo-Neto, D. M. A. Melo, R. M. Braga and M. A. F. Melo, *Fuel*, 2021, **287**, 119511.
64 S. Baskar, S. Yuvaraj, P. S. Subudhi, M. Sundararajan and D. Chandra Sekhar, *J. Chin. Chem. Soc.*, 2021, **68**, 630–638.
65 C. B. Palan, N. S. Bajaj, S. P. Bhagat and S. K. Omanwar, *Luminescence*, 2021, **36**, 1491–1497.
66 S. A. Ansari, C. Manjunatha, N. Parveen, B. W. Shivaraj and R. H. Krishna, *Dalton Trans.*, 2021, **50**, 14891–14907.
67 S. Kanithan, N. A. Vignesh, K. M. Katubi, P. S. Subudhi, E. Yanmaz, J. A. Dhanraj, N. S. Alsaiari, k. M. Abualnaja, M. Sukumar, M. Sundararajan, S. Baskar, S. Sahu and C. S. Dash, *J. Mol. Struct.*, 2022, **1265**, 133289.
68 A. T. Dhiwahar, S. Maruthamuthu, K. V. Chandekar, M. S. Hamdy, M. Shkir, M. Sundararajan and P. Sakthivel, *Adv. Powder Technol.*, 2021, **32**, 4030–4041.
69 M. Sertkol, Y. Köseoğlu, A. Baykal, H. Kavas, A. Bozkurt and M. S. Toprak, *J. Alloys Compd.*, 2009, **486**, 325–329.
70 M. R. D. Freitas, G. L. D. Gouveia, L. J. Dalla Costa, A. J. A. D. Oliveira and R. H. G. A. Kiminami, *Mater. Res.*, 2016, **19**, 27–32.
71 S. Chamani, M. Khatamian, N. S. Peighambardoust and U. Aydemir, *ACS Omega*, 2021, **6**, 33024–33032.
72 E. Carlos, R. Martins, E. Fortunato and R. Branquinho, *Chem.–Eur. J.*, 2020, **26**, 9099–9125.
73 E. Mahu, P. Samoila, M. Ignat, C. Cojocaru and V. Harabagiu, *Cron. Chim.*, 2022, **25**, 189–202.
74 S. Rasouli, A. M. Arabi, A. Naeimi and S. M. Hashemi, *J. Fluoresc.*, 2018, **28**, 167–172.
75 A. Khort, K. Podbolotov, R. Serrano-García and Y. Gun'ko, *Inorg. Chem.*, 2018, **57**, 1464–1473.
76 H. Nayebzadeh, N. Saghatoleslami and M. Tabasizadeh, *J. Nanostruct. Chem.*, 2019, **9**, 141–152.
77 M. Derakhshani, E. Taheri-Nassaj, M. Jazirehpour and S. M. Masoudpanah, *J. Alloys Compd.*, 2021, **886**, 161195.
78 K. Frikha, S. Bennici, J. Bouaziz, K. Chaari and L. Limousy, *Energies*, 2020, **13**, 3126.
79 M. Radpour, S. Alamolhoda and S. M. Masoudpanah, *Ceram. Int.*, 2017, **43**, 13729–13734.
80 P. Araichimani, K. Prabu, G. S. Kumar, G. Karunakaran, S. Surendhiran, M. Shkir and H. E. Ali, *Ceram. Int.*, 2022, **48**, 10339–10345.
81 R. O. Yathisha and Y. Arthoba Nayaka, *Russ. J. Electrochem.*, 2021, **57**, 784–794.
82 M. Hashemzehi, V. Pirouzfar, H. Nayebzadeh and A. Alihosseini, *Fuel*, 2020, **263**, 1–14.